ChemComm

COMMUNICATION

View Article Online
View Journal | View Issue

Cite this: *Chem. Commun.*, 2015, 51, 4693

Received 6th December 2014,
Accepted 6th February 2015

DOI: 10.1039/c4cc09760b

www.rsc.org/chemcomm

A new O3-type layered oxide cathode with high energy/power density for rechargeable Na batteries†

Haodong Liu,‡[a] Jing Xu,‡[ab] Chuze Ma[a] and Ying Shirley Meng*[a]

A new O3–$Na_{0.78}Li_{0.18}Ni_{0.25}Mn_{0.583}O_w$ is prepared as the cathode material for Na-ion batteries, delivering exceptionally high energy density and superior rate performance. The single-slope voltage profile and *ex situ* synchrotron X-ray diffraction data demonstrate that no phase transformation happens through a wide range of sodium concentrations (up to 0.8 Na removed). Ni^{2+}/Ni^{4+} is suggested to be the main redox center. Further optimization could be realized by tuning the combination and the ratio of transition metals.

Na-ion batteries have recently gained increasing recognition as intriguing candidates for next-generation large scale energy storage systems, owing to significant cost advantages stemming from the high natural abundance and broad distribution of Na resources.

For the past several years, a variety of novel materials have been explored as electrodes for Na-ion batteries. Since the Na ion has a relatively larger ionic radius than that of the Li ion, materials with an open framework are required for facile Na ion insertion/extraction. Following this strategy, many breakthroughs in cathode materials have been achieved.[1,2] Among most of the Na cathode compounds, the P2 and O3 structured Na oxides (Na_xTMO_2, TM = transition metal) have drawn significant attention, since their relatively opened structures are able to accommodate large Na ions providing spacious diffusion path as well as the structural stability. The research on Na_xTMO_2 was started in the 70's by Delmas *et al.*[3,4] Recently, various P2-Na_xTMO_2, and their binary or ternary derivatives, have been extensively investigated and some of them demonstrated superior electrochemical performances.[5–11] On the other hand, O3 structured materials have also shown a great progress. For example, $NaCrO_2$ was investigated by Komaba *et al.*, and showed 120 mA h g^{-1} of specific capacity near 2.9 V.[12,13] O3–$NaNi_{0.5}Mn_{0.5}O_2$ electrodes delivered 105 mA h g^{-1} at 1C (240 mA g^{-1}) and 125 mA h g^{-1} at C/30 (8 mA g^{-1}) in the voltage range of 2.2–3.8 V and displayed 75% of the capacity after 50 cycles.[13,14] The Fe-substituted O3–$Na[Ni_{1/3}Fe_{1/3}Mn_{1/3}]O_2$ exhibited the specific capacity of 100 mA h g^{-1} with an average operating voltage at 2.75 V.[15] The isostructural compound, $Na[Ni_{1/3}Mn_{1/3}Co_{1/3}]O_2$, showed reversible intercalation of 0.5 Na-ions leading to the specific capacity of 120 mA h g^{-1} in the voltage range of 2.0–3.75 V.[16] These relatively low capacity and limited cycling retention are presumably due to the fact that most of these materials undergo multiple phase transformations from O3 to O′3, P3, P′3 and then P″3 consecutively.[17] These transformations could be one of the major problems that limit the practical use of Na-ion batteries since they deteriorate the cycle life and rate capabilities. Herein, to overcome this issue, a new O3 compound is prepared through Li–Na ion exchange, inspired by the idea in Li-ion batteries that a Li-excess O3 compound has demonstrated a single slope voltage profile with significant improvement in capacity and cycling retention for Li layered electrodes.[18–20]

$Li_{1.133}Ni_{0.3}Mn_{0.567}O_2$ was synthesized by heating a mixture of $LiOH{\cdot}H_2O$ and $Ni_{0.346}Mn_{0.654}(OH)_2$ (for Experimental details, see ESI†). The obtained $Li_{1.133}Ni_{0.3}Mn_{0.567}O_2$ was firstly charged in the Li half cell to extract Li ions (the composition at this point is $Li_{0.073}Ni_{0.3}Mn_{0.567}O_w$) and then discharged in the Na half cell to prepare O3–$Na_{0.719}Li_{0.073}Ni_{0.3}Mn_{0.567}O_w$ (Fig. S1, ESI†). To achieve higher capacity, the ratio among Li, Ni and Mn was further adjusted and the composition, $Li_{1.167}Ni_{0.25}Mn_{0.583}O_2$, was finally chosen, which improved the initial Na-insertion capacity from 220 mA h g^{-1} to 240 mA h g^{-1}. Fig. 1a illustrates the electrochemical profiles for the initial "delithiation" (Li-extraction) and "sodiation" (Na-extraction) processes for $Li_{1.167}Ni_{0.25}Mn_{0.583}O_2$. The initial "delithiation" of Li-excess material showed a long plateau at 4.5 V which involved oxygen loss (and/or oxidation). The stoichiometry for the ion-exchanged material is $Na_{0.78}Li_{0.18}Ni_{0.25}Mn_{0.583}O_w$, as determined by the electrochemical capacity and energy-dispersive X-ray spectroscopy. We used subscript w ($0 < w < 2$) in the formula to describe the oxygen loss during initial charge. The as-prepared $Na_{0.78}Li_{0.18}Ni_{0.25}Mn_{0.583}O_w$ has a particle size less than 500 nm (Fig. S2, ESI†). The cycling performance is

[a] *Department of NanoEngineering, University of California San Diego, 9500 Gilman Drive, La Jolla, CA 92093, USA. E-mail: shirleymeng@ucsd.edu; Fax: +858-534-9553; Tel: +858-822-4247*

[b] *Environmental Energy Technologies Division, Lawrence Berkeley National Laboratory, Berkeley, CA 94720, USA*

† Electronic supplementary information (ESI) available. See DOI: 10.1039/c4cc09760b

‡ These two authors contributed equally.

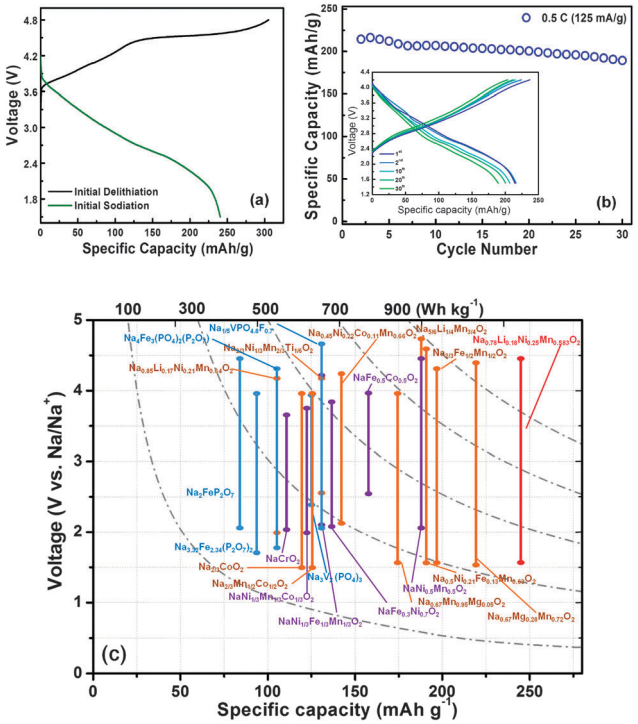

Fig. 1 (a) Electrochemical profiles of initial delithiation and initial sodiation for $Na_{0.78}Li_{0.18}Ni_{0.25}Mn_{0.583}O_w$ in half cell. (b) Cycling performance of $Na_{0.78}Li_{0.18}Ni_{0.25}Mn_{0.583}O_w$ with 125 mA g^{-1} current density. The inset is the corresponding electrochemical profile of $Na_{0.78}Li_{0.18}Ni_{0.25}Mn_{0.583}O_w$ during the 1st, 2nd, 10th, 20th, and 30th cycles in Na-ion batteries. (c) Comparison of reversible capacities for the intercalation-based Na cathodes.[24–46]

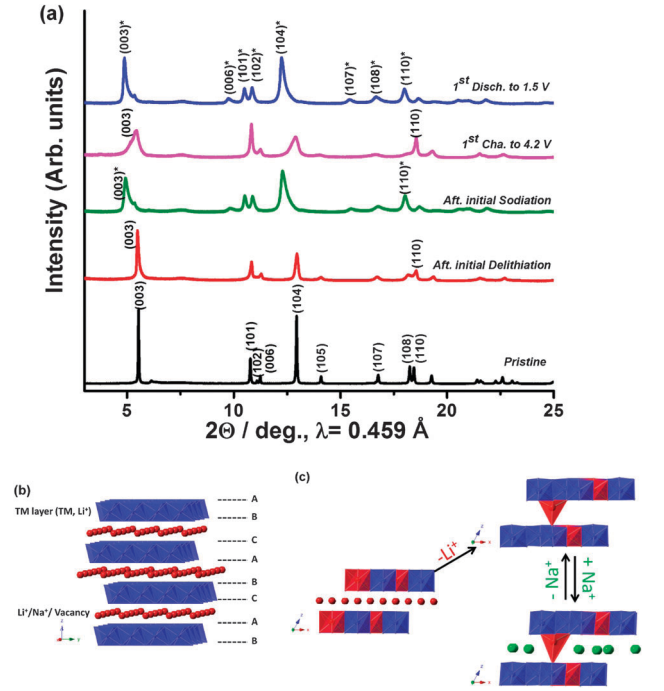

Fig. 2 (a) *Ex situ* SXRD of $Li_{1.167}Ni_{0.25}Mn_{0.583}O_2$ and $Na_{0.78}Li_{0.18}Ni_{0.25}Mn_{0.583}O_w$ at different states. (b) Schematic of the typical O3 structure. (c) Schematic of the proposed mechanism for sodiation. (In the schematic, transition metal ions are blue, Li^+ is red, and Na^+ is green.)

tested between 1.5 and 4.2 V with a current density at 125 mA g^{-1}. After 30 cycles, around 190 mA h g^{-1} capacity is well maintained as shown in Fig. 1b. With 1.25 A g^{-1} current, the reversible capacity is still as high as 160 mA h g^{-1}, suggesting its high-power capability (Fig. S3, ESI†). Fig. 1c compares capacity and energy density for most of the recent cathodes in Na-ion batteries (highest reversible value is selected). $Na_{0.78}Li_{0.18}Ni_{0.25}Mn_{0.583}O_w$ exhibits not only the highest capacity but also the highest energy density: 675 W h kg^{-1} energy density is delivered by this material during discharge, which is higher than the recent results reported by Kataoka *et al.* who used a similar ion exchange method,[21] and even higher than $LiFePO_4$ (560 W h kg^{-1}) and $LiCoO_2$ (560 W h kg^{-1}) in Li-ion batteries.[22–24] More interestingly, as displayed in the inset of Fig. 1b, no voltage steps are seen in the electrochemical profiles upon cycling. It indicates the no phase transformations happen for this O3 material even after all the Na ions are extracted. Besides, the voltage depression problem, which is usually observed in its parent material, $Li_{1.167}Ni_{0.25}Mn_{0.583}O_2$ in Li-ion batteries,[47] is reduced to some degree in this ion-exchanged product in Na-ion batteries.

The synchrotron X-ray diffraction (SXRD) was conducted at selected states of charge/discharge to detect the structural change (Fig. 2a). The refined lattice parameters are summarized in Table S1, ESI.† As shown with the black line in Fig. 2a, the as-synthesized material, $Li_{1.167}Ni_{0.25}Mn_{0.583}O_2$, is well crystallized and can be indexed as an $R\bar{3}m$ space group. The diffraction pattern illustrates typical Li-excess features, which have been discussed in our previous work.[47] After initial delithiation (red line in Fig. 2a), the *c* lattice is slightly increased (Table S1, ESI†) due to less screening effects between neighboured oxygen layers when Li ions are mostly removed from the host.[48] Upon initial sodiation (green line in Fig. 2a), the whole spectrum is significantly shifted to a lower angle, such as (003) and (110) peaks. The shift is resulted from the overall lattice expansion, as the inserted Na ions have much large ionic size than Li ions. Peak broadening is observed, which is probably ascribed to the stacking faults introduced during initial sodiation. The small reflection to the right of the (003) peak is from the non-reacted residue Li compound phase. More work is underway to comprehensively investigate this process. It should be noted that although the diffraction peaks are moved systematically, all the peaks still belong to the $R\bar{3}m$ space group, in other words, an O3 phase (Fig. 2b), proving that there is no change in the host structure during the ion-exchange process. To further monitor the electrode structural change upon cycling in Na batteries, two *ex situ* samples were characterized. When the electrode is charged to 4.2 V (pink line in Fig. 2a), the material still maintains an O3 structure though the majority of Na ions are removed as suggested by charging capacity. Upon comparing with the material after initial sodiation, it is interesting to notice that the (003) peak is moved to a higher angle, indicating that the *c* lattice is reduced at this state. Moreover, all the peak positions are close to those of the material after initial delithiation. Since Li moving to tetrahedral sites after first charge has been extensively observed in Li-ion batteries,[47–49] it is hypothesized that the tetrahedral Li would form similarly in our initial delithiation process as shown in Fig. 2c. These tetrahedral Li ions play a critical role in stabilizing the O3 phase at subsequent cycles by locking the neighboured layer shifting. When the electrode is discharged to 1.5 V (blue line in Fig. 2a), the spectrum is back to the similar

positions with the material after initial sodiation, suggesting that the Na ions are re-inserted back. And most importantly, the O3 phase is still well maintained.

In order to investigate the charge compensation mechanism during Na-ion extraction and insertion, X-ray absorption spectroscopy (XAS) measurements were conducted with Ni and Mn K-edges at different states of charge. Normalized Ni and Mn K-edge X-ray absorption near edge structure (XANES) spectra are shown in Fig. 3a and b, respectively. For the standards, Ni K-edge spectra of divalent Ni-ion (NiO) and Mn K-edge spectra of tetravalent Mn-ion (MnO_2) are included. It is evident that an as-synthesized $Li_{1.167}Ni_{0.25}Mn_{0.583}O_2$ compound predominantly consists of Ni^{2+} and Mn^{4+}. Obvious changes are shown in the Ni XANES spectra upon initial delithiation, sodiation, and followed by the charge and discharge process. The Ni K-edge absorption energy of an initially delithiated electrode shifts to the higher energy region compared to that of the as-synthesized state. The amount of absorption energy shift is $\sim$3 eV, suggesting that the oxidation state of Ni after initial delithiation is close to Ni^{4+}.[47] After initial sodiation, the oxidation state of Ni ions returns back to divalent. The similar edge shift and recovery are seen again between 4.2 V and 1.5 V in *ex situ* electrode samples suggesting that the Ni^{2+}/Ni^{4+} redox reaction is completely reversible in Na-ion batteries. In contrast to the Ni XANES, Mn K-edge XANES shows that Mn ions mainly stay at the tetravalent state and no dramatic changes occur in the valence upon charge and discharge. The subtle variations in the edge shape and the position in XANES could be attributed to surface reaction of the particle, which has been reported in its Li analogue[50] and requires more advanced characterization to investigate. Based on the Ni and Mn XANES, it is proved that Ni is the only electrochemically active species and Mn supports the structural stability in the absence of Jahn–Teller active Mn^{3+}. More details on local structural change are revealed by the extended X-ray absorption fine structure (EXAFS) spectra. Ni EXAFS clearly shows that interatomic distances of Ni–O and Ni–TM are shortened after initial delithiation and after the charge in Na-ion batteries, indicating that the oxidation of Ni ions. After initial sodiation, the interatomic distances are systematically larger than the as-synthesized state, resulting from lattice expansion when Na ions are inserted. However, Mn EXAFS does not show any significant change in the Mn–O interatomic distance (small changes may be due to the local environment changes), although the second shell corresponding to the Mn–TM distance is varied with different voltages. This is ascribed to the changes in the Ni oxidation states, which accordingly affect the distance among neighboured Mn–Ni.

To evaluate the practical application of $Na_{0.78}Li_{0.18}Ni_{0.25}Mn_{0.583}O_w$, the full cell was fabricated with $Na_{0.78}Li_{0.18}Ni_{0.25}Mn_{0.583}O_w$ as a cathode and SnS_2/rGO as an anode. (Fig. 4a) The anode is reported in our previous work.[51] In our full cell configuration, both cathode materials and anode materials are casted on an Al current collector, which will further reduce the cost and weight of the Na ion battery. Fig. 4b presents voltage profiles of the full cell with a discharge capacity of $\sim$210 mA h g^{-1} (capacity based on cathode weight). The overall capacity of Na full cell using our advanced cathode and anode can reach 175 mA h g^{-1} (considering the weight of cathode and anode materials). The operation discharge voltage is on average 2.5 V. As a result, the total energy density for this Na full cell is as high as 430 W h kg^{-1}, which is to our best knowledge the highest energy so far reported for Na full cells. Furthermore, the capacity is well maintained for this Na full cell. As shown in Fig. 4c, after 50 cycles, more than 165 mA h g^{-1} is delivered reversibly.

In fact, the ion-exchange electrode performance could be further adjusted by mixing with other TM, such as Co. As shown in Fig. S4a (ESI†), if the parent Li compound is designed with Co in the stoichiometry as $Li_{1.167}Ni_{0.166}Mn_{0.5}Co_{0.166}O_2$, the discharged capacity is further increased to 245 mA h g^{-1}. In addition, the direct synthesis route has been tried preliminarily. The as-synthesized material, $NaLi_{0.067}Co_{0.267}Ni_{0.267}Mn_{0.4}O_2$, has demonstrated a pure O3 phase. However, the direct synthesis by the co-precipitation method will be hard to create tetrahedral Li, we

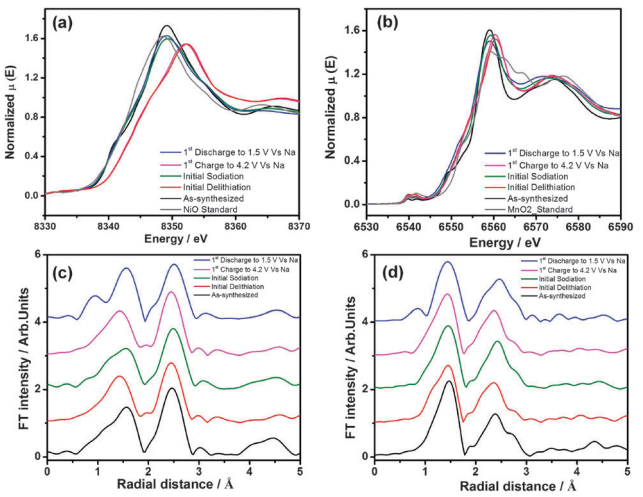

Fig. 3 XAS analysis of $Li_{1.167}Ni_{0.25}Mn_{0.583}O_2$ and $Na_{0.78}Li_{0.18}Ni_{0.25}Mn_{0.583}O_w$ at different states. XANES spectra of (a) Ni and (b) Mn K-edges respectively. EXAFS spectra of (c) Ni and (d) Mn K-edges respectively.

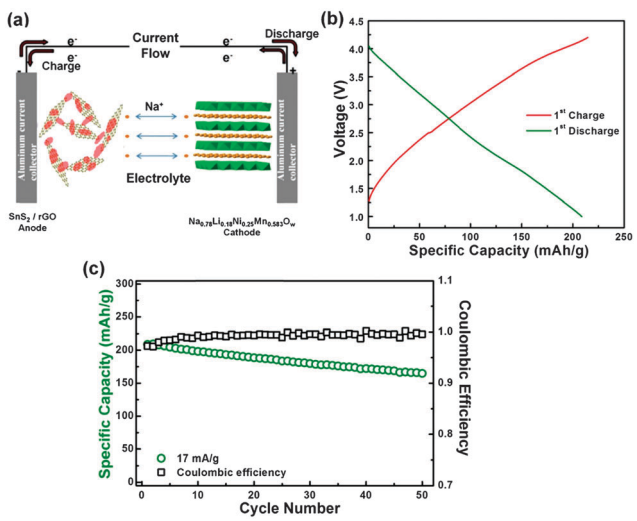

Fig. 4 (a) Schematic of Na full cell. (b) The electrochemical profile at 1st cycle and (c) cycling performance of the Na full cell.

cannot exclude the possibilities from the other method, and more efforts are made now.

In conclusion, a new O3–$Na_{0.78}Li_{0.18}Ni_{0.25}Mn_{0.583}O_w$ is obtained by the electrochemical Na–Li ion exchange process of $Li_{1.167}Ni_{0.25}Mn_{0.583}O_2$. The new material shows exceptionally a high discharge capacity of 240 mA h g^{-1} in the voltage range of 1.5–4.5 V, thus the total energy density of the material level reaches 675 W h kg^{-1}. It is the highest capacity as well as the highest energy density so far among all the reported cathodes in Na-ion batteries. When cycled between 1.5–4.2 V, the discharge capacity is well maintained at around 190 mA h g^{-1} after 30 cycles. The O3 phase is maintained through an ion-exchange and cycling process, as confirmed by SXRD. The stabilized O3 phase could be related to the tetrahedral Li formed upon initial lithiation, and breaks through the critical limitation for most of the O3 compounds. XAS results show that Ni^{2+}/Ni^{4+} is the main active redox couple during cycling while Mn ions basically stay at the tetravalent state. The Na full cell utilizing $Na_{0.78}Li_{0.18}Ni_{0.25}Mn_{0.583}O_w$ as a cathode delivers 430 W h kg^{-1} energy density, shedding light on the future of Na-ion technologies. Future improvement could be realized through fine tuning the combination and the ratio among TMs, and making the material by direct synthesis, which will be reported very soon.

Haodong Liu and Jing Xu equally contributed to this work. The authors are grateful for the financial support from the Northeastern Center for Chemical Energy Storage, an Energy Frontier Research Center funded by the U.S. Department of Energy, Office of Basic Energy Sciences, with Award Number DE-SC0012583. H. Liu acknowledges the financial support from China Scholarship Council under Award Number 2011631005. The authors appreciate the kind assistance from Dr Baihua Qu for anode SnS_2/rGO synthesis at National University of Singapore (NUS). The XAS and SXRD were collected on 20-BM-B and 11-BM respectively at Advanced Photon Source in Argonne National Laboratory.

References

1 J. Xu, D. H. Lee and Y. S. Meng, *Funct. Mater. Lett.*, 2013, **6**, 1330001.
2 M. R. Palacin, *Chem. Soc. Rev.*, 2009, **38**, 2565–2575.
3 C. Delmas, C. Fouassier and P. Hagenmuller, *Physica B+C*, 1980, **99**, 81–85.
4 C. Fouassier, C. Delmas and P. Hagenmuller, *Mater. Res. Bull.*, 1975, **10**, 443–449.
5 J. Xu, D. H. Lee and Y. S. Meng, *Funct. Mater. Lett.*, 2013, **6**, 1330001.
6 R. Berthelot, D. Carlier and C. Delmas, *Nat. Mater.*, 2011, **10**, U73–U74.
7 D. H. Lee, J. Xu and Y. S. Meng, *Phys. Chem. Chem. Phys.*, 2013, **15**, 3304–3312.
8 H. Yoshida, N. Yabuuchi, K. Kubota, I. Ikeuchi, A. Garsuch, M. Schulz-Dobrick and S. Komaba, *Chem. Commun.*, 2014, **50**, 3677–3680.
9 Z. Jie, X. Jing, L. Dae Hoe, N. Dimov, Y. S. Meng and S. Okada, *J. Power Sources*, 2014, **264**, 235–239.
10 S. W. Kim, D. H. Seo, X. H. Ma, G. Ceder and K. Kang, *Adv. Energy Mater.*, 2012, **2**, 710–721.
11 D. Kim, S. H. Kang, M. Slater, S. Rood, J. T. Vaughey, N. Karan, M. Balasubramanian and C. S. Johnson, *Adv. Energy Mater.*, 2011, **1**, 333–336.
12 S. Komaba, C. Takei, T. Nakayama, A. Ogata and N. Yabuuchi, *Electrochem. Commun.*, 2010, **12**, 355–358.
13 S. Komaba, T. Nakayama, A. Ogata, T. Shimizu, C. Takei, S. Takada, A. Hokura and I. Nakai, *ECS Trans.*, 2009, **16**, 43–55.
14 S. Komaba, N. Yabuuchi, T. Nakayama, A. Ogata, T. Ishikawa and I. Nakai, *Inorg. Chem.*, 2012, **51**, 6211–6220.
15 D. Kim, E. Lee, M. Slater, W. Lu, S. Rood and C. S. Johnson, *Electrochem. Commun.*, 2012, **18**, 66–69.
16 M. Sathiya, K. Hemalatha, K. Ramesha, J.-M. Tarascon and A. S. Prakash, *Chem. Mater.*, 2012, **24**, 1846–1853.
17 M. Ati, L. Dupont, N. Recham, J. N. Chotard, W. T. Walker, C. Davoisne, P. Barpanda, V. Sarou-Kanian, M. Armand and J. M. Tarascon, *Chem. Mater.*, 2010, **22**, 4062–4068.
18 Y. Gao and J. R. Dahn, *J. Electrochem. Soc.*, 1996, **143**, 100–114.
19 J. S. Kim, C. S. Johnson, J. T. Vaughey, M. M. Thackeray and S. A. Hackney, *Chem. Mater.*, 2004, **16**, 1996–2006.
20 N. Yabuuchi, K. Yoshii, S. T. Myung, I. Nakai and S. Komaba, *J. Am. Chem. Soc.*, 2011, **133**, 4404–4419.
21 R. Kataoka, T. Mukai, A. Yoshizawa and T. Sakai, *J. Electrochem. Soc.*, 2013, **160**, A933–A939.
22 J. M. Tarascon and M. Armand, *Nature*, 2001, **414**, 359–367.
23 J. B. Goodenough and Y. Kim, *Chem. Mater.*, 2010, **22**, 587–603.
24 B. L. Ellis, K. T. Lee and L. F. Nazar, *Chem. Mater.*, 2010, **22**, 691–714.
25 H. Yoshida, N. Yabuuchi, K. Kubota, I. Ikeuchi, A. Garsuch, M. Schulz-Dobrick and S. Komaba, *Chem. Commun.*, 2014, **50**, 3677–3680.
26 N. Yabuuchi, M. Kajiyama, J. Iwatate, H. Nishikawa, S. Hitomi, R. Okuyama, R. Usui, Y. Yamada and S. Komaba, *Nat. Mater.*, 2012, **11**, 512–517.
27 N. Yabuuchi, M. Yano, H. Yoshida, S. Kuze and S. Komaba, *J. Electrochem. Soc.*, 2013, **160**, A3131–A3137.
28 N. Yabuuchi, M. Kajiyama, J. Iwatate, H. Nishikawa, S. Hitomi, R. Okuyama, R. Usui, Y. Yamada and S. Komaba, *Nat. Mater.*, 2012, **11**, 512–517.
29 D. Kim, E. Lee, M. Slater, W. Q. Lu, S. Rood and C. S. Johnson, *Electrochem. Commun.*, 2012, **18**, 66–69.
30 D. Kim, S.-H. Kang, M. Slater, S. Rood, J. T. Vaughey, N. Karan, M. Balasubramanian and C. S. Johnson, *Adv. Energy Mater.*, 2011, **1**, 333–336.
31 X. F. Wang, M. Tamaru, M. Okubo and A. Yamada, *J. Phys. Chem. C*, 2013, **117**, 15545–15551.
32 P. Barpanda, G. Liu, C. D. Ling, M. Tamaru, M. Avdeev, S.-C. Chung, Y. Yamada and A. Yamada, *Chem. Mater.*, 2013, **25**, 3480–3487.
33 P. Barpanda, J. Lu, T. Ye, M. Kajiyama, S.-C. Chung, N. Yabuuchi, S. Komaba and A. Yamada, *RSC Adv.*, 2013, **3**, 3857–3860.
34 P. Barpanda, T. Ye, S. Nishimura, S. C. Chung, Y. Yamada, M. Okubo, H. S. Zhou and A. Yamada, *Electrochem. Commun.*, 2012, **24**, 116–119.
35 K. H. Ha, S. H. Woo, D. Mok, N. S. Choi, Y. Park, S. M. Oh, Y. Kim, J. Kim, J. Lee, L. F. Nazar and K. T. Lee, *Adv. Energy Mater.*, 2013, **3**, 770–776.
36 K. Saravanan, C. W. Mason, A. Rudola, K. H. Wong and P. Balaya, *Adv. Energy Mater.*, 2013, **3**, 444–450.
37 J. Y. Jang, H. Kim, Y. Lee, K. T. Lee, K. Kang and N.-S. Choi, *Electrochem. Commun.*, 2014, **44**, 74–77.
38 H. Kim, Y.-U. Park, K.-Y. Park, H.-D. Lim, J. Hong and K. Kang, *Nano Energy*, 2014, **4**, 97–104.
39 Y. U. Park, D. H. Seo, H. S. Kwon, B. Kim, J. Kim, H. Kim, I. Kim, H. I. Yoo and K. Kang, *J. Am. Chem. Soc.*, 2013, **135**, 13870–13878.
40 H. Kim, I. Park, S. Lee, H. Kim, K.-Y. Park, Y.-U. Park, H. Kim, J. Kim, H.-D. Lim, W.-S. Yoon and K. Kang, *Chem. Mater.*, 2013, **25**, 3614–3622.
41 H. Kim, I. Park, D. H. Seo, S. Lee, S. W. Kim, W. J. Kwon, Y. U. Park, C. S. Kim, S. Jeon and K. Kang, *J. Am. Chem. Soc.*, 2012, **134**, 10369–10372.
42 K. Saravanan, C. W. Mason, A. Rudola, K. H. Wong and P. Balaya, *Adv. Energy Mater.*, 2013, **3**, 444–450.
43 M. Sathiya, K. Hemalatha, K. Ramesha, J.-M. Tarascon and A. S. Prakash, *Chem. Mater.*, 2012, **24**, 1846–1853.
44 H. Yoshida, N. Yabuuchi and S. Komaba, *Electrochem. Commun.*, 2013, **34**, 60–63.
45 N. Yabuuchi, R. Hara, K. Kubota, J. Paulsen, S. Kumakura and S. Komaba, *J. Mater. Chem. A*, 2014, **2**, 16851–16855.
46 J. Billaud, G. Singh, A. R. Armstrong, E. Gonzalo, V. Roddatis, M. Armand, T. Rojo and P. G. Bruce, *Energy Environ. Sci.*, 2014, **7**, 1387–1391.
47 B. Xu, C. R. Fell, M. Chi and Y. S. Meng, *Energy Environ. Sci.*, 2011, **4**, 2223–2233.
48 H. D. Liu, C. R. Fell, A. Ke, C. Lu and Y. S. Meng, *J. Power Sources*, 2013, **240**, 772–778.
49 D. Mohanty, J. L. Li, D. P. Abraham, A. Huq, E. A. Payzant, D. L. Wood and C. Daniel, *Chem. Mater.*, 2014, **26**, 6272–6280.
50 K. J. Carroll, D. Qian, C. Fell, S. Calvin, G. M. Veith, M. F. Chi, L. Baggetto and Y. S. Meng, *Phys. Chem. Chem. Phys.*, 2013, **15**, 11128–11138.
51 B. H. Qu, C. Z. Ma, G. Ji, C. H. Xu, J. Xu, Y. S. Meng, T. H. Wang and J. Y. Lee, *Adv. Mater.*, 2014, **26**, 3854–3859.

